Colloids and Surfaces B: Biointerfaces 136 (2015) 134–140

Contents lists available at ScienceDirect

Colloids and Surfaces B: Biointerfaces

journal homepage: www.elsevier.com/locate/colsurfb

Multimodal imaging probe for targeting cancer cells using uMUC-1 aptamer

Won Jun Kang[a,1], Jonghwan Lee[b,c,1], Yong Seung Lee[b,c], Sujeong Cho[b,c], Bahy A. Ali[d,e], Abdulaziz A. Al-Khedhairy[f], Hyejung Heo[b,c], Soonhag Kim[b,c,*]

[a] Division of Nuclear Medicine, Department of Radiology, Yonsei University College of Medicine, Republic of Korea
[b] Institute for Bio-Medical Convergence, College of Medicine, Catholic Kwandong University, Gangneung-si, Gangwon-do 270-701, Republic of Korea
[c] Catholic Kwandong University International St. Mary's Hospital, Incheon Metropolitan City 404-834, Republic of Korea
[d] Al-Jeraisy DNA Research Chair, Department of Zoology, College of Science, King Saud University, Riyadh 11451, Saudi Arabia
[e] Department of Nucleic Acids Research, Genetic Engineering and Biotechnology Research Institute, City for Scientific Research and Technological Applications, Alexandria, Egypt
[f] Department of Zoology, College of Science, King Saud University, Riyadh 11451, Saudi Arabia

ARTICLE INFO

Article history:
Received 25 April 2015
Received in revised form 16 July 2015
Accepted 1 September 2015
Available online 5 September 2015

Keywords:
Aptamer
Nanoparticle
Multimodal imaging
Cancer
uMUC-1

ABSTRACT

For adequate cancer therapy, newer imaging modalities with more specific ligands for unique targets are crucial. Underglycosylated mucin-1 (uMUC-1) antigen is an early marker of tumor development and is widely overexpressed on most tumors. A combination of nanotechnology with optical, radionuclide, and magnetic resonance (MR) imaging has great potential to improve cancer diagnosis and therapy. In this study, a multimodal nanoparticle imaging system was developed that can be used for optical, MR and positron emission tomography (PET) imaging. Cobalt ferrite magnetic nanoparticles surrounded by fluorescent rhodamine (designated MF) within a silica shell matrix were conjugated with an aptamer targeting uMUC-1 (designated MF-uMUC-1) and further labeled by ^{68}Ga (designated MFR-uMUC-1) with the help of a *p*-SCN-bn-NOTA chelating agent, resulting in single multimodal nanoparticles. The resultant nanoparticles are spherical and monodispersed, as revealed by transmission electron microscopy. The MFR-uMUC-1 nanoparticle showed specific and dose-dependent fluorescent, radioisotope and MR signals targeting BT-20 cells expressing uMUC-1. *In vivo* targeting and multimodal imaging in tumor-bearing nude mice also showed great specificity for targeting cancers with MFR-uMUC-1. The MFR-uMUC-1 probe could be used as a single multimodal probe to visualize cancer cells by means of optical, radionuclide and MR imaging.

1. Introduction

Clinical anatomical medical imaging modalities including computed tomography (CT) and magnetic resonance imaging (MRI) have been used in the diagnosis of many cancers [1]. Fluorodeoxyglucose (FDG) positron emission tomography (PET) is one of the major imaging modalities in oncology, and was recently used to determine the degree of glucose metabolism in cancer cells [2]. FDG-PET, CT and MRI were successfully applied in targeting several tumors with low glucose metabolism [3]. However, a highly specific tumor-targeting molecular imaging probe is essential to diagnose cancers at an earlier stage. The ability to image molecular and genetic changes is of great value. Antibodies are widely used to target specific cellular signals, but have limitations such as hypersensitivity response, long serum half-life and difficulties in production. An aptamer is a small synthetic oligonucleotide that binds to a specific target with high affinity and specificity. The advantages of using an aptamer over antibiotic agents include a lack of immunogenicity, small size and ease of synthesis [4,5]. Several aptamers have been developed for targeting cancer-specific proteins such as nucleolin, vascular endothelial growth factor (VEGF), and prostate specific membrane antigens (PSMA) [6–8]. Furthermore, aptamers labeled with radioisotope or quantum dot have shown potential as imaging ligands [9,10].

Molecular imaging plays an important role in non-invasive visualization of molecular process and cellular function, and is

* Corresponding author at: Institute for Bio-Medical Convergence, College of Medicine, Catholic Kwandong University, International St. Mary's Hospital, Republic of Korea.
E-mail address: kimsoonhag@empal.com (S. Kim).
[1] These authors contributed equally to this work.

http://dx.doi.org/10.1016/j.colsurfb.2015.09.004
0927-7765/

emerging as a highly promising tool to detect disease and improve treatment [11]. Recent progress in molecular imaging has been reinforced by recent advancements in nanotechnology techniques. One example of nanotechnology-based molecular imaging is the development of multifunctional nanoparticles conjugated with specific ligands such as antibodies, aptamers, peptides, and small molecules that bind to specific targets [12–14]. Imaging modalities such as optical, bioluminescence, MRI and PET are the most widely used, each with unique advantages and disadvantages. Fluorescence imaging has been widely used for *in vitro* and *in vivo* cellular imaging with great convenience. However, due to high autofluorescence and poor tissue penetration, the utility of *in vivo* fluorescence imaging is limited. Bioluminescence has low autofluorescence and a higher lesion-to-background ratio. However, it requires genetic modification and has limited tissue penetration. Contrary to optical imaging methods, nuclear and MR imaging can visualize deep signals, which is the reason these two modalities have been used clinically. Nuclear imaging is more sensitive than MR, but image resolution is better with MR than with PET. A multimodal imaging approach has been suggested to overcome the limitations of each modality. Initial multimodal approaches focused on hybrid imaging such as PET-CT, PET-MR and MR-optical [15,16]. However, a more detailed localization of biologic processes can be obtained using a multimodal imaging probe, which allows visualization of different imaging signals from optical, radioisotope and MR simultaneously. Several multimodal imaging probes have been used for monitoring cancers or stem cells [17–19].

Here, we developed a cancer-targeting multimodal nanoparticle probe using an aptamer that can be utilized to detect cancers with fluorescence, radionuclide and MR imaging. The aptamer was selected to target underglycosylated mucin-1 (uMUC-1), which is highly expressed by the majority of adenocarcinomas [20,21].

2. Materials and methods

2.1. Manufacturing MF nanoparticle

MNP@SiO_2(RITC)-(PEG)/COOH/pro-N/NH_2 nanoparticles (MF) containing carboxyl moieties (1.1×10^4/nanoparticle) were purchased from Biterials (Seoul, Republic of Korea). The method used to generate the multimodal nanoparticle cancer probe with an aptamer was performed as previously described [19]. Cobalt ferrite magnetic particles were mixed with a poly-vinyl pyrrolidone (PVP, Sigma, St. Louis, MO) solution. After stabilization with PVP solution, the cobalt-ferrite particles were centrifuged at 4000 rpm for 10 min with acetone. Trimethoxysilane modified by fluorescent dye RITC was prepared from aminopropyltriethoxysilane (ASP) and RITC. The reaction mixture of tetraethoxysilane (TEOS) and synthesized dye was injected into PVP-stabilized cobalt ferrite particles. By adding an ammonia solution as a catalyst, polymerization was initiated resulting in RITC-trapped silica-coated magnetic nanoparticles (MNP@SiO_2(RITC), MF). MNP@SiO_2(RITC)-PEG/NH_2 was formed by adding an amino and PEGylated group to the surface of MNP@SiO_2(RITC).

2.2. Construction of the MF-uMUC-1 probe

uMUC-1 aptamer was purchased from Bionics (BIONICS, Seoul, Korea). The uMUC-1 aptamer sequence was as follows: 5′-NH_2-GGGAGACAAGAATAAACGCTCAAGCAGT.

TGATCCTTTGGATACCCTGGTTCGACAGGAGGCTCACAACAGGC-3′. The uMUC-1 mutant (uMUC-1 mt) was manufactured with random nucleotide sequences for comparison. The uMUC-1 mt aptamer sequence was as follows: 5′-NH_2-TGCTTCGTTGAGAACTCACA.

ATTTAACAACAGAGGACATAAGCCCTACGCCCATGATCTACTGA-CGTCCCTG-3′.

The MF-uMUC-1 probe was obtained by covalent conjugation of carboxyl moieties of MF particle with a 5′-NH_2 modified uMUC-1 aptamer using *N*-(3-dimethylaminoproppyl)-*N*-ethylcarbodiiamide (EDC) (MF: uMUC-1 aptamer molar ratio, 1:3) for 1 h at room temperature. The MF-uMUC-1 conjugates were washed by centrifugation at 15,000 rpm for 10 min and suspended in buffer solution (50 mM Tris–HCl, pH 7.4). The conjugation efficiency between MF particle carboxyl groups and uMUC-1 amine groups of the aptamer was calculated by collecting each unconjugated probe from the supernatant after centrifugation of the MF conjugate and measuring the concentration using a NanoDrop ND-1000 Spectrometer (NanoDrop products, Wilmington, DE, USA). These data are presented as the mean ± standard deviation (SD) calculated from quadruple wells.

2.3. Morphological analysis of the MF-uMUC-1 nanoparticle

Transmission electron microscopy (TEM) of MF, MF-uMUC-1, and MF-uMUC-1 mt nanoparticles ($n = 3$) was performed using a JEM 1010 (JEOL, Japan) at 80 kV. Each nanoparticle was fixed using 2% formaldehyde for 10 min. Samples were prepared by placing one drop of a dilute solution of each nanoparticle in methanol onto a copper grid supporting a thin plastic film and then removing the remaining solvent after 2 min by applying a hot air flux. High-resolution electron microscope digital images were recorded with a Gatan-cooled CCD camera. Dynamic light scattering was conducted to measure the size of MF, MF-uMUC-1, and MF-uMUC-1 mt nanoparticles ($n = 3$) (Zetasizer Nano ZS system Malvern Instruments, Worcestershire, UK).

2.4. Cell culture

BT-20 (a human breast cancer cell line) and Chinese hamster ovary (CHO) cells and L132 human lung epithelial cells were purchased from the Korea Cell Line Bank (Seoul, Korea). Sertoli TM4 cells were purchased from the American Type Culture Collection (ATCC). BT-20, CHO, L132 and TM4 cells were maintained in DMEM (Gibco, Grand Island, NY) supplemented with 10% fetal bovine serum (FBS, Invitrogen, Grand Island, NY), 10 U/ml penicillin (Invitrogen, Grand Island, NY), and 10 μg/ml streptomycin. The cells were split at regular intervals.

2.5. MTT assay

BT-20 cells were seeded onto a 24-well plate at a density of 2×10^5/well overnight and then treated with various concentrations of the MF, NF-uMUC-1 and MF-uMUC-1 mt (0, 50, 100, 250 and 500 pM, $n = 3$) for 24 h. A total of 2 mg/ml of 3-(4,5-dimethythazolzyl)-2,5-diphenyletrazolium bromide (MTT) solution was added to each well (50 μl/well) and incubated for 4 h at 37 °C. The supernatant was then discarded and the precipitate was dissolved in 500 ml of DMSO, after which the plates were read on a microplate reader (Tecan Spectra, Wetzlar, Germany) at 540 nm. The viability of cells was calculated based on a comparison of untreated cells and those treated with MTT under the same conditions.

2.6. Western blot analysis

Quantification of uMUC-1 expression in BT-20 cells was measured by Western blot analysis. BT-20, CHO, L132 and TM4 cells were lysed in a buffer containing 10 mM Tris–HCl (pH 7.5), 1 mM DTT, 20% glycerol, 1 mM EDTA, and protease inhibitor mixture. Protein concentrations were determined using BCA protein kits (Pierce,

Rockford, IL), and the resulting lysates were cleared by centrifugation. Membranes were blocked in TBS-T (20 mM Tris, 137 mM NaCl, 0.1% Tween 20) containing 3% nonfat dried milk and incubated with MUC-1 antibody (1:5000 dilution, Abcam, UK) or beta-actin antibody (1:5000 dilution, Sigma, St. Louis, MO) for 120 min. The membranes were then washed three times with TBS-T, and anti-mouse IgG (H + L) was added. Immunochemical detection was performed using WEST-zol (plus) (intron, Seongnam-si, Gyeonggi-do, Korea) with a Las 3000.

2.7. Confocal microscopy

Cells (1×10^5) were plated on sterile coverslips in a 24-well plate. After rinsing with PBS twice, either MF-uMUC-1 or MF-uMUC-1 mt probe was incubated with cells. After incubation for 4 h at 37 °C, cells were fixed with gentle shaking for 20 min in 3.7% formaldehyde solution (Sigma, St. Louis, MO). Cells were then washed three times with PBS for 10 min and cover-slipped with a mounting medium containing 4′,6-diamidino-2-phenylindole dihydrochloride (DAPI) solution (Vector Laboratories, Inc., CA). Confocal images were acquired by confocal laser scanning microscopy (Carl Zeiss LSM 510, Weimer, Germany) with excitation and emission wavelengths of 558 and 581 nm, respectively.

2.8. In vitro *fluorescence analysis*

BT-20 cells were seeded onto a 24-well plate at a density of 1×10^5 cells per well, then incubated in a 5% CO_2 humidified chamber for 24 h. The cells were subsequently incubated at 4 °C for 30 min to decrease non-specific binding. Either MF-uMUC-1 or MF-uMUC-1mt particles were applied to BT-20 cells under serum-free conditions. The samples were incubated at 4 °C for 30 min, and then washed twice for 10 min at RT with mild shaking. The cells were then lysed with RIPA buffer (Thermo Fisher Scientific Inc., Waltham, MA), and were transferred into dark 96-well microplates (Chemicell GmbH, Germany). Fluorescence intensity was measured using Infinite M200 (Tecan, GmbH, SZ, Austria) with a scanning wavelength of 558/581 nm. All data are presented as the mean ± SD calculated from quadruple wells, and significant differences between samples were assessed using the Student's *t*-test ($P < 0.05$).

2.9. Labeling MF-uMUC-1 with ^{68}Ga to produce MFR-uMUC-1 particles and in vitro experiments with BT-20 cells

The MF-uMUC-1 conjugates were washed by centrifugation at 22,250 rpm for 10 min and suspended in buffer solution (50 mM Tris–HCl, pH 7.4). After 1 h of incubation, MF-uMUC-1 was washed twice with Tris buffer (pH 7.4) and briefly sonicated. Binding of MF with *p*-SCN-bn-NOTA (2-(*p*-isothiocyanatobezyl)-1,4,7-triazacyclonane-1,4,7-triacetic acid, 500 $g mol^{-1}$, concentration 5 mg/ml) adduct was performed at a reaction ratio of 1:5 (MF:NOTA). The reaction was performed in $NAHCO_3$ buffer solution (pH 9) under vortex with mild shaking at 4 °C overnight. To label MF-NOTA with ^{68}Ga, $^{68}GaCl_3$ was eluted from a $^{68}Ge/^{68}Ga$ generator using 4 ml of 0.1 M HCl (432.9 MBq, 11.7 mCi/4 ml). The $^{68}GaCl_3$ activity used for the *in vitro* experiments was 37 MBq (1 mCi/340 μl). The reaction mixture was prepared by mixing MF-NOTA with $^{68}GaCl_3$ adjusted to a pH of 6.5 with 0.2 M Na_2HPO4/NaH_2PO4 buffer (Sigma, St. Louis, MO), and incubated for 1 h after brief vortexing. To monitor the labeling efficiency of MF by ^{68}Ga, thin layer chromatography (TLC) was performed at each incubation time point. The reaction mixture was separated using ITLC-SG (Instant TLC-silica gel) (Pall, Inc., Michigan) using a 0.1 M citric acid solvent, and radioactivity was measured using an AR-2000 TLC imaging scanner (Bioscan, Inc., Washington, DC). The ^{68}Ga labeling efficiency was measured and expressed as percentage by region of interest (ROI) measurement of ITLC-SG.

2.10. Magnetic resonance analysis

BT-20 cells (5×10^5) were treated with MF-uMUC-1 or MF-uMUC-1 mt at five different concentrations (0, 25, 50, 100 and 200 pM). After washing three times with PBS, cells were detached by trypsin/EDTA. The detached cells were then fixed with 4% paraformaldehyde. The T2-weighted MR images with a fast low-angle shot sequences were acquired using 1.5T MRI (GE Medical system, Milwaukee, WI).

2.11. In vivo *cancer targeting and multimodal imaging*

BT-20 cells (1×10^6 cells) were harvested in PBS buffer and incorporated within a PLLA scaffold. The cell-scaffold complexes were implanted into the right thighs of nude mice. The left thighs were implanted with a cell-free PLLA scaffold as a control. The implanted cells were cultured for 3 weeks until the tumors reached 100–200 mm^3 in volume. Then, MFR-uMUC-1 or MF-uMUC-1 mt were intravenously (IV) injected into the tumor-bearing nude mice *via* the tail vein ($n = 6$). For image scanning, all mice were anesthetized with 1% isoflurane-O_2 air. For *in vivo* dynamic positron emission tomography (PET) images, a small-animal PET/CT scanner (eXplore Vista; GE Healthcare) was used, and images were acquired over 10 min. ROI analysis was performed by selecting the areas of implanted right and left thighs on the images. The average number of counts per pixel was measured for both thighs. The *in vivo* Fluorescence images were obtained using IVIS®-200 spectrum imaging system (Caliper Life Sciences, MA). *In vivo* MR images were obtained using a 3T clinical MRI instrument with a micro-47 surface coil (Intera; Philips Medical Systems, Best, Netherlands). The T2-weighted MR images were measured using the T2 Turbo Spin Echo sequences at room temperature with the following parameters: TR = 4000 ms, TE = 114 ms, and slice thickness = 1.0 mm.

2.12. Statistical analysis

Data are presented as the mean ± standard deviation and were analyzed using the Student's *t*-test. *P* values less than 0.05 and 0.005 were considered statistically significant.

3. Results

3.1. Construction of the MFR-uMUC-1 particle as a tumor targeting probe

We used a magnetic-fluorescent-radioisotope (MFR) nanoparticle, magnetic fluorescence nanoparticle (MF) and MNP@SiO_2(RITC)-(PEG)/COOH/pro-N/NH_2 to construct a multimodal imaging probe. The MF particle was composed of magnetic cobalt ferrite in the central core and rhodamine B isothiocyanate fluorescence dye (RITC, excitation/emission = 555/578 nm) coated with a silica shell [18]. Polyethylene glycol (PEG) (1×10^4/nanoparticle), Fmoc-protected amine moieties, and a carboxyl group surrounded the surface of the MF particles, and was labeled with the MUC-1 aptamer and *p*-SCN-bn-NOTA chelator. The MF nanoparticles were covalently conjugated with the uMUC-1 aptamer or uMUC-1 mutant oligonucelotide (uMUC-1 mt) with a molar ratio of 1:3 for 1 h at room temperature using the coupling reagent EDC (*N*-(3-dimethylaminopropyl)-*N*′-ethyl-carbodiimide hydrochloride, 40 nM) (Fig. 1). Transmission electron microscopy (TEM) images showed that the MF, MF-uMUC-1 and

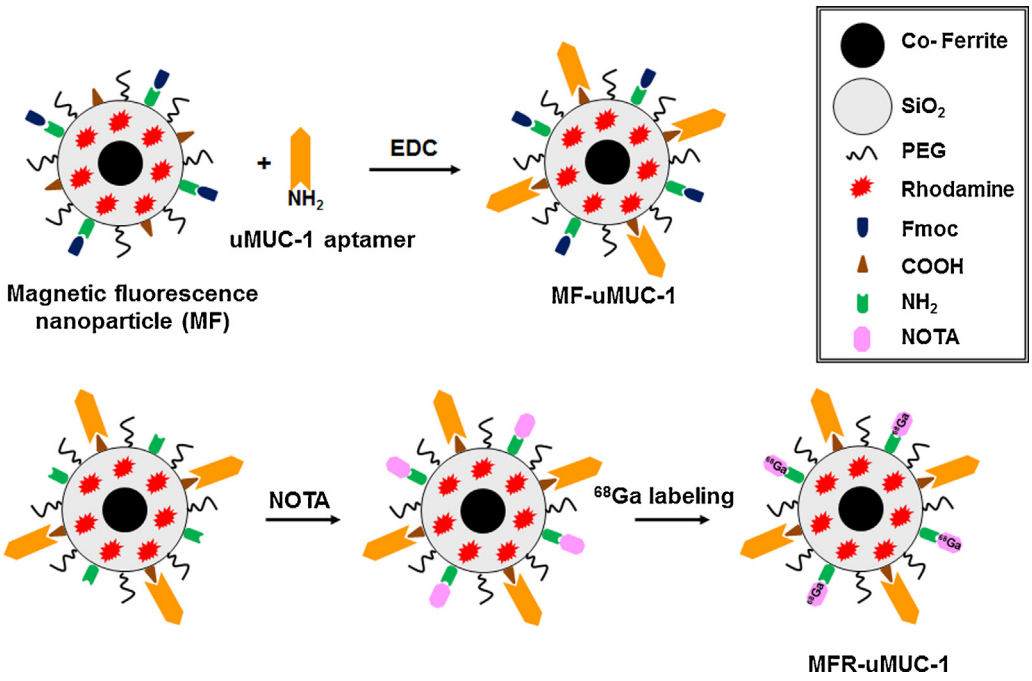

Fig. 1. Schematic illustration of MFR-uMUC-1 probe synthesis. The MF particle has carboxyl group and Fmoc-protected amine moiety, which was conjugated with amine-terminated uMUC-1 aptamer (MF-uMUC-1). ^{68}Ga was labeled with the MF-uMUC-1 to form the MFR-uMUC-1 after reaction with *p*-SCN-bn-NOTA.

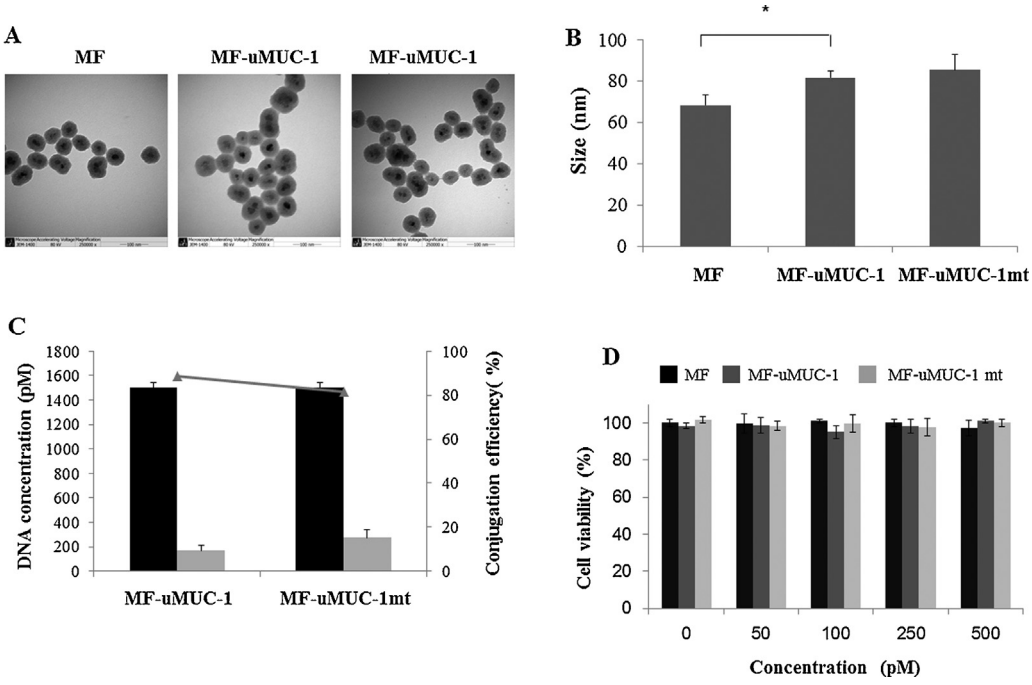

Fig. 2. Characteristics of the MF-uMUC-1. (A) TEM images of MF, MF-uMUC-1 and MF-uMUC-1 mt. The scale bar = 100 nm. (B) DLS analysis of MF, MF-uMUC-1 and MF-uMUC-1 mt. The data are displayed as the mean ± SD. $^*P < 0.05$. (C) Conjugation efficiency of the MF with uMUC-1 aptamer or uMUC-1 mt oligonucleotide. The *x*-axis indicates the DNA concentration (1500 pM) of uMUC-1 or uMUC-1 mt used for conjugation with the MF (black bar), and unconjugated and remained in the supernatant after centrifugal filtration (gray bar). The *y*-axis represents the percentage of conjugation efficiency (gray line with triangle head) acquired by percentage of one minus decoupling efficiency. These data were presented as the mean ± SD calculated from quadruple wells. (D) MTT assay of the MF, MF-uMUC-1 and MF-uMUC-1 mt in BT-20 cells. There was no observed significant reduction in cell viability with various concentrations (0, 50, 100, 250, and 500 pM).

MF-uMUC-1 mt nanoparticles had monodispersed spherical shape and were crystalline (Fig. 2A). Dynamic light scattering (DLS) analysis demonstrated that the sizes of the MF, MF-uMUC-1 and MF-uMUC-1 mt particles were approximately 68, 81, and 85 nm, respectively (Fig. 2B). Successful formation of MF-uMUC-1 or MF-uMUC-1 mt was confirmed by a slight increase in diameter of the MF nanoparticle after conjugation with the uMUC-1 aptamer or uMUC-1 mt. The coupling efficiency of the MF nanoparticle (0.5 nM) was 88.5% for uMUC-1 aptamer (1.5 nM) and 81.4% for uMUC-1 mt (1.5 nM) (Fig. 2C). To validate the toxicity of the

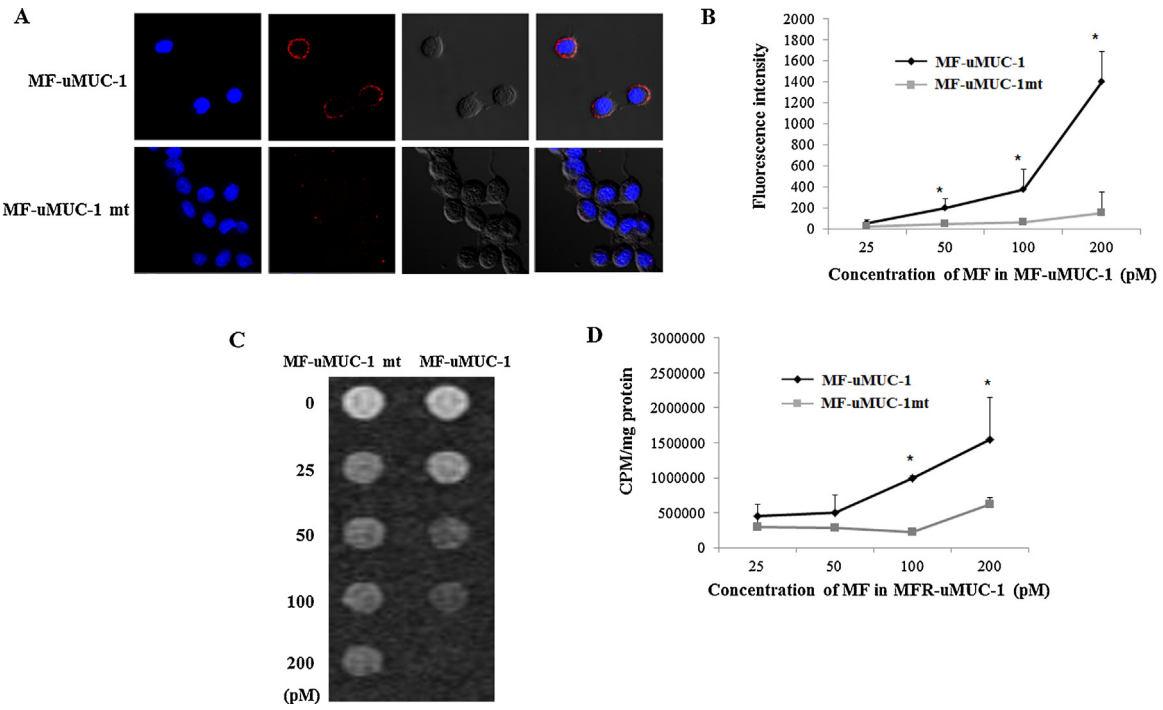

Fig. 3. Multimodal imaging of the MFR-uMUC-1 probe for targeting BT-20 cells. The molar ratio for the conjugation of MF or MFR with uMUC-1 or uMUC-1 mt was 1:3. (A) Confocal microscopy image of the MF-uMUC1 in BT-20 cells. Fluorescence signals with the MF-uMUC-1 (100:300 pM) were found along the cellular surface of BT-20 cells, suggesting specific binding of the MF-uMUC-1 to BT-20 cells. No fluorescence signal was noted in BT-20 cells using the MF-uMUC-1 mt (100:300 pM). Column 1 shows DAPI imaging (nucleus); column 2: rhodamine fluorescence signal in MF; column 3: cellular morphology; column 4: merged image. Gradually increased concentrations of uMF-uMUC-1, MF-uMUC-1 mt, MFR-uMUC-1, MFR-uMUC-1 mt were incubated with BT-20 cells for 1 h. Dramatic differences in fluorescence (B), magnetic resonance (C) and radioisotope (D) signals in targeting BT-20 cells were found from the multimodal imaging probe conjugated with uMUC-1 compared with MUC-1 mt. These data are presented as the mean ± SD calculated from quadruple wells. $^{*}P < 0.05$.

nanoparticles, various concentrations of MF, MF-uMUC-1 and MF-uMUC-1 mt particles were incubated with BT-20 cells. Incubation with the nanoparticles did not affect cell viability (Fig. 2D).

3.2. Affinity of MF-uMUC-1 in BT-20 cells

To conduct multimodal imaging of the targeting cancer using the MFR-uMUC-1 nanoparticle, BT-20 cells were incubated with serially increasing concentrations of the MF-uMUC-1 particle. Western blot analysis demonstrated that uMUC-1 was highly expressed in BT-20 cells compared with three normal cell lines that do not express uMUC-1, L132 human lung epithelial cells, TM4 cells and CHO cells (Supplementary Fig. S1). For confocal microscopy analysis of targeting cancers was achieved by adding multimodal nanoparticle-conjugated uMUC-1, MF-uMUC-1 or MF-uMUC-1 mt to BT-20 cells and three normal cell lines, L132 cells, TM4 cells and CHO cells. The MF-uMUC-1 showed strong rhodamine fluorescence brightness in BT-20 cells (Fig. 3A), while no fluorescence signals were detected in three normal cell lines (Supplementary Fig. S2). Interestingly, significant fluorescence brightness was found along the plasma membrane of the BT-20 cells. Our confocal microscopy finding validated the cellular membrane distribution of uMUC-1 [22]. There was no fluorescence signal detected in the plasma membranes of the MF-uMUC-1 mt- treated BT-20 cells. To investigate the quantitative fluorescence intensities of the MF-uMUC-1 nanoparticles targeting cancer, 1×10^5 BT-20 cells were incubated at 4 °C for 30 min to decrease non-specific binding. Optical targeting intensity from BT-20 cells was measured with gradually increased concentrations of the MF-uMUC-1 particles. The results showed that the MF-uMUC-1-treated BT-20 cells revealed a dose-dependent and significant increase in fluorescence intensity (Fig. 3B). However, the MF-uMUC-1 mt-treated BT-20 cells showed no significant difference in fluorescence intensity as the concentration of the MF-uMUC-1 mt increased gradually. These results represent the high specificity of the MF-uMUC-1 particle for targeting BT-20 cells.

To investigate the clinical possibility of targeting cancer using the prepared MF-uMUC-1 probe, phantom MR images of BT-20 cells were acquired. Five different concentrations (0, 25, 50, 100 and 200 pM) of either MF-uMUC-1 or MF-uMUC-1 mt were incubated with BT-20 cells for 1 h. The T2-weighted MR images at 1.5T showed a gradual decrease in the magnetic signal intensity from BT-20 cells in proportion to serial increase in MF-uMUC-1 concentration (Fig. 3C). The specific relaxivity was 8.533 $mM^{-1}\,s^{-1}$ (Supplementary Fig. S3). In contrast, no difference in MR intensities were observed from BT-20 cells as the concentration of the MF-uMUC-1 mt increased.

To examine the clinical feasibility of targeting BT-20 cells with the multimodal imaging probe conjugated with the uMUC-1 aptamer, an Fmoc-protection group was removed from the MF-uMUC-1 nanoparticle and then labeled with ^{68}Ga-citrate using a NOTA chelator to form the MFR-uMUC-1 (Fig. 1). Quantitative thin layer chromatography (TLC) analysis demonstrated that approximately 32.1% of the MFR-uMUC-1 incorporated ^{68}Ga-citrate (Supplementary Fig. S4). After labeling with ^{68}Ga-citrate using NOTA chelator, BT-20 cells were treated with MFR-uMUC-1 at various concentrations (MF particle, 25, 50, 100 and 200 pM) for 1 h. The radionuclide activity using a γ-scintillation counter demonstrated that ^{68}Ga radioactivity in BT-20 cells was gradually and significantly increased when compared with MFR-uMUC-1 mt as the concentration of MFR-uMUC-1 increased (Fig. 3D). The radionuclide activity of MFR-uMUC-1 was significantly higher at 100 and 200 pM when compared to MFR-uMUC-1 mt.

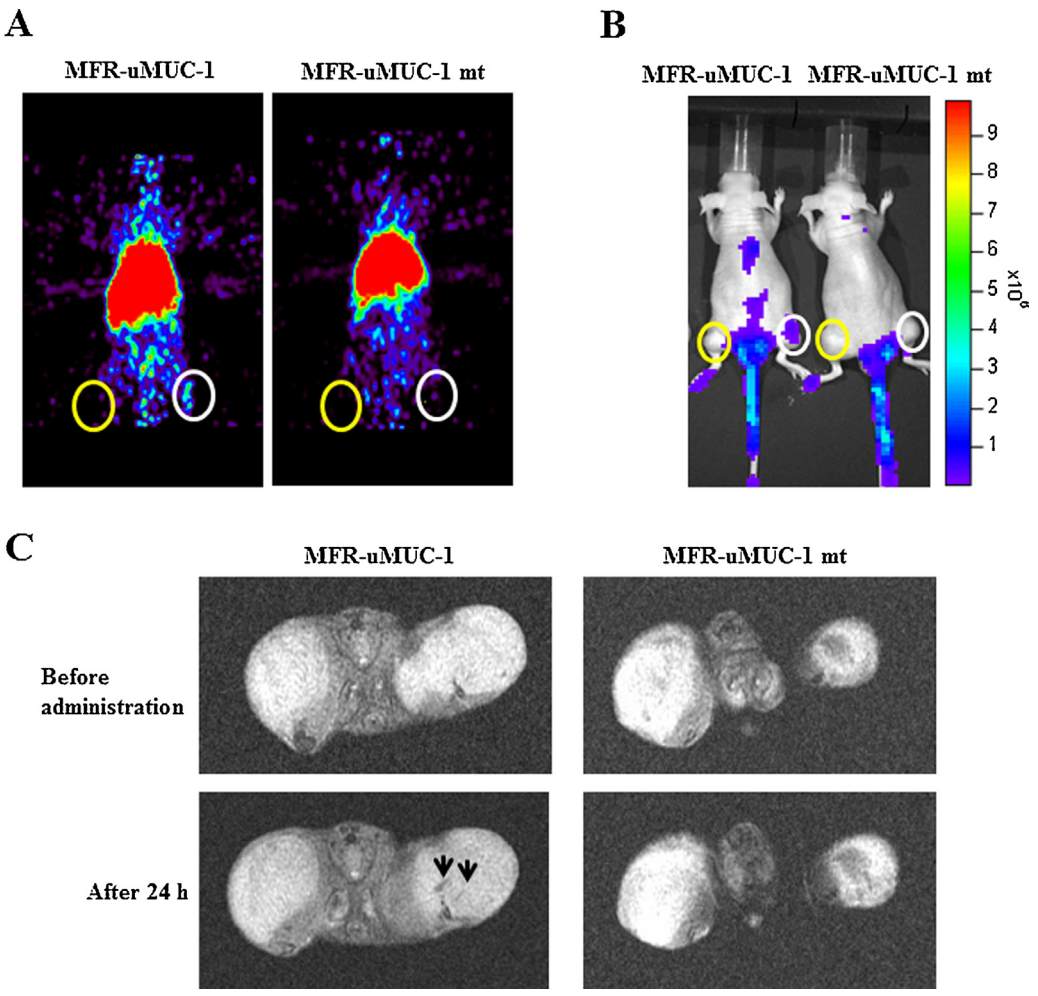

Fig. 4. *In vivo* multimodal imaging analysis for cancer targeting. The BT-20 cell-PLLA scaffold complexes were implanted into the right thighs (white circles) and scaffolds without BT-20 cells were implanted into the left thighs (yellow circles) of nude mice, respectively. MFR-uMUC-1 or MFR-uMUC-1 mt were injected intravenously (IV) into the tumor-bearing nude mice ($n = 6$). After IV injection, targeting signals were detected only from the right thighs of the MFR-uMUC-1-injected mice. (A) Dynamic small-animal PET images showed increased ^{68}Ga radioactivity. (B) *In vivo* fluorescence image showed high fluorescence intensity. (C) The T2-weighted MR image showed a dark signal (black arrow). No signals were detected in the left thighs of nude mice or in the right thighs of the MFR-uMUC-1 mt-injected nude mice. (For interpretation of the references to color in this figure legend, the reader is referred to the web version of this article.)

3.3. In vivo *cancer targeting and multimodal imaging*

For *in vivo* multimodal cancer imaging, BT-20 cells were incorporated within a PLLA scaffold and implanted into the right thighs of nude mice. The left thighs were administered with the PLLA scaffold without BT-20 cells. Then, MFR-uMUC-1 or MF-uMUC-1 mt was intravenously (IV) injected into tumor-bearing mice. Radionuclide images were obtained at 2 h after IV injection. The dynamic small-animal PET image showed increased ^{68}Ga radioactivity from the right thigh of MFR-uMUC-1-injected mice (Fig. 4A). Quantitative ROI analysis further confirmed showed the higher ^{68}Ga radioactivity in the right thigh of MFR-uMUC-1-injected group than that of in the left thigh and those of MFR-uMUC-1 mt-injected group in both thighs (Supplementary Fig. S5). The high fluorescence signal was detected 12 h after injection from the right thigh of MFR-uMUC-1-injected mice (Fig. 4B). The detected signals from outside the tumors were resulted from the non-specific retention of nanoparticles. Such non-specific retention is usually detected in liver, spleen and lung mainly because of the mononuclear phagocytic system (MPS), and the clearance of circulating nanoparticles from the bloodstream in mice is also occur [23,24]. The MFR-uMUC-1 mt-administered mice showed rapid clearance through the bloodstream, indicating that the MFR-uMUC-1 specifically targeted the tumors. The MR images of other mice were obtained before and 24 h after injection. The T2-weighted MR images showed decreased dark signals from the right thigh of MFR-uMUC-1-injected mice (Fig. 4C). However, there were no significant signals in fluorescence, radioactivity and MR intensity in the left thighs of nude mice containing only the PLLA scaffold or in the right thighs of MFR-uMUC-1 mt-injected nude mice. These results demonstrated a high specificity for targeting cancers expressing uMUC-1 *in vivo*.

4. Discussion

In recent years, multimodal imaging platforms with dual or triple moieties, including reporter genes or nanoparticles, have gained popularity [25–27]. With multimodal imaging, one modality can complement another, which is useful for overcoming the limitations of a single imaging modality. For example, PET or MR imaging for human application should be preceded by testing successful optical probes in animal imaging. However, transforming optical probes into PET or MR probes can cause structural alteration, changing the probes' affinity and distribution. In addition, direct comparison of two different images is difficult due to limitations in resolution and position changes. In order to overcome these modality-specific limitations, a single imaging probe developed to

be used with multiple imaging modalities would have a promising future in both basic and clinical research.

In this study, we successfully demonstrated a multimodal imaging probe for *in vitro* and *in vivo* cancer targeting with the MFR-uMUC-1 nanoparticle by means of optical, radionuclide and MR imaging of the same mouse. Triple imaging modalities demonstrated that the MFR-uMUC-1 probe had great specificity for targeting uMUC-1 expressed in BT-20 cells when compared to the MFR-uMUC-1 mt probe. In addition, the pattern of quantitative optical imaging for targeting BT-20 cells using the MFR-uMUC-1 nanoparticle was successfully reproduced by other clinical imaging modalities, radionuclides and MRI. This suggests MFR-uMUC-1 could be used in a single imaging probe for targeting cancer that would allow *in vivo* triple imaging modalities. For clinical application, our multimodal probe should be improved in simultaneous imaging. The different modalities were imaged and collected separately according to each modality. In addition, for long-term PET imaging, additional radionuclide generators having relatively long half-lives need to be applied.

5. Conclusion

We developed the MFR-uMUC-1 nanoparticles for targeting and multimodal imaging of cancer in BT-20 cells. The MFR-uMUC-1 nanoparticles successfully targeted MUC-1 in BT-20 cells with high affinity and visualized uMUC-1 by optical, radionuclide, and MRI modalities. The MFR-uMUC-1 particle as multimodal imaging platform offers a novel and powerful approach to visualizing cancer cells *in vivo*. A diverse variation of MF particles with different aptamers for various targets and imaging moieties will provide a platform to greatly improve cancer diagnosis and treatment.

Acknowledgements

This work was supported by the Bio & Medical Technology Development Program of the National Research Foundation (NRF) funded by the Korean Government (MEST) (No. 2013R1A2A2A01068140), the Next-Generation BioGreen 21 program (#PJ010002), Rural Development Administration and a grant of the Korean Health Technology R&D Project, Ministry of Health & Welfare (HI14C3297), and the Visiting Professor Program (VPP) at King Saud University, Kingdom of Saudi Arabia.

Appendix A. Supplementary data

Supplementary data associated with this article can be found, in the online version, at http://dx.doi.org/10.1016/j.colsurfb.2015.09.004.

References

[1] R. Weissleder, M.J. Pittet, Imaging in the era of molecular oncology, Nature 452 (2008) 580–589.
[2] D.J. Margoli, J.M. Hoffman, R.J. Herfkens, R.B. Jeffrey, A. Quon, S.S. Gambhir, Molecular imaging techniques in body imaging, Radiology 245 (2007) 333–356.
[3] T.C. Kwee, S. Basu, B. Saboury, V. Ambrosini, D.A. Torigian, A. Alavi, A new dimension of FDG-PET interpretation: assessment of tumor biology, Eur. J. Nucl. Med. Mol. Imaging 38 (2011) 1158–1170.
[4] H. Shi, X. He, K. Wang, X. Wu, X. Ye, Q. Guo, W. Tan, Z. Qinq, X. Yang, B. Zhou, Activatable aptamer probe for contrast-enhanced *in vivo* cancer imaging based on cell membrane protein-triggered conformation alteration, Proc. Natl. Acad. Sci. U. S. A. 108 (2011) 3900–3905.
[5] Y. Pu, Z. Zhu, H. Liu, J. Zhang, J. Liu, W. Tan, Using aptamers to visualize and capture cancer cells, Anal. Bioanal. Chem. 397 (2010) 3225–3233.
[6] E.M. Reyes-Reyes, Y. Teng, P.J. Bates, A new paradigm for aptamer therapeutic AS1411 action: uptake by macropinocytosis and its stimulation by a nucleolin-dependent mechanism, Cancer Res. 70 (2010) 8617–8629.
[7] A.S. Potty, K. Kourentzi, H. Fang, G.W. Jackson, X. Zhang, G.B. Legge, R.C. Willson, Biophysical characterization of DNA aptamer interactions with vascular endothelial growth factor, Biopolymers 91 (2009) 145–156.
[8] K. Min, H. Jo, K. Song, M. Cho, Y.S. Chun, S. Jon, W.J. Kim, C. Ban, Dual-aptamer-based delivery vehicle of doxorubicin to both PSMA (+) and PSMA (−) prostate cancers, Biomaterials 32 (2011) 2124–2132.
[9] B.J. Hicke, A.W. Stephens, T. Gould, Y.F. Chang, C.K. Lynott, J. Heil, S. Borkowski, C.S. Hilger, G. Cook, S. Warren, P.G. Schmidt, Tumor targeting by an aptamer, J. Nucl. Med. 47 (2006) 668–678.
[10] A.K. Cheng, H. Su, Y.A. Wang, H.Z. Yu, Aptamer-based detection of epithelial tumor marker mucin 1 with quantum dot-based fluorescence readout, Anal. Chem. 81 (2009) 6130–6139.
[11] J.K. Willmann, N. van Bruggen, L.M. Dinkelborg, S.S. Gambhir, Molecular imaging in drug development, Nat. Rev. Drug. Discov. 7 (2008) 507–591.
[12] A. Toma, E. Otsuji, Y. Kuriu, K. Okamoto, D. Ichikawa, A. Hagiwara, H. Ito, T. Nishimura, H. Yamagishi, Monoclonal antibody A7-superparamagnetic iron oxide as contrast agent of MR imaging of rectal carcinoma, Br. J. Cancer 93 (2005) 131–136.
[13] O.C. Farokhzad, J. Cheng, B.A. Teply, I. Sherifi, S. Jon, P.W. Kantoff, J.P. Richie, R. Langer, Targeted nanoparticle-aptamer bioconjugates for cancer chemotherapy in vivo, Proc. Natl. Acad. Sci. U. S. A. 103 (2006) 6315–6320.
[14] W.J. Gradishar, S. Tjulandin, N. Davidson, H. Shaw, N. Desai, P. Bhar, M. Hawkins, J. O'Shaughnessy, Phase III trial of nanoparticle albumin-bound paclitaxel compared with polyethylated castor oil-based paclitaxel in women with breast cancer, J. Clin. Oncol. 53 (2005) 7794–7803.
[15] W. Cai, X. Chen, Nanoplatforms for targeted molecular imaging in living subjects, Small 3 (2007) 1840–1854.
[16] G. Antoch, A.J. Bockisch, Combined PET/MRI: a new dimension in whole-body oncology imaging? Eur. J. Nucl. Med. Mol. Imaging 36 (2009) S113–S120.
[17] M. Doubrovin, I. Serganova, P. Mayer-Kuckuk, V. Ponomarev, R.G. Blasberg, Multimodality *in vivo* molecular-genetic imaging, Bioconjug. Chem. 15 (2004) 1376–1388.
[18] D.W. Hwang, H.Y. Ko, J.H. Lee, H. Kang, S.H. Ryu, I.C. Song, D.S. Lee, S. Kim, A nucleolin-targeted multimodal nanoparticle imaging probe for tracking cancer cells using an aptamer, J. Nucl. Med. 51 (2010) 98–105.
[19] H.Y. Ko, K.J. Choi, C.H. Lee, S. Kim, A multimodal nanoparticle-based cancer imaging probe simultaneously targeting nucleolin, integrin αvβ3 and tenascin-C proteins, Biomaterials 32 (2011) 1130–1138.
[20] A. Ohgami, T. Tsuda, T. Osaki, T. Mitsudomi, Y. Morimoto, T. Higashi, K. Yasumoto, MUC1 mucin mRNA expression in stage I lung adenocarcinoma and its association with early recurrence, Ann. Thorac. Surg. 67 (1999) 810–814.
[21] K. Tsuta, G. Ishii, J. Nitadori, Y. Murata, T. Kodama, K. Nagai, A. Ochiai, Comparison of the immunophenotypes of signet-ring cell carcinoma, solid adenocarcinoma with mucin production, and mucinous bronchioloalveolar carcinoma of the lung characterized by the presence of cytoplasmic mucin, J. Pathol. 209 (2006) 78–87.
[22] M. Brayman, A. Thathiah, D.D. Carson, MUC1: a multifunctional cell surface component of reproductive tissue epithelia, Reprod. Biol. Endocrinol. 2 (2004) 4.
[23] E. Ruoslahti, S.N. Bhatia, M.J. Sailor, Targeting of drugs and nanoparticles to tumors, JCB 188 (2010) 759–768.
[24] V.J. Mohanraj, Y. Chen, Nanoparticles —a review, Trop. J. Pharm. Res. 5 (2006) 561–573.
[25] W. Wang, S. Ke, S. Kwon, S. Yallampalli, A.G. Cameron, A.E. Adams, M.E. Mawad, E.M. Sevick-Muraca, A new optical and nuclear dual-labeled imaging agent targeting interleukin 11 receptor alpha-chain, Bioconjug. Chem. 18 (2007) 397–402.
[26] P. Ray, A. De, J.J. Min, R.Y. Tsien, S.S. Gambhir, Imaging tri-fusion multimodality reporter gene expression in living subjects, Cancer Res. 64 (2004) 1323–1330.
[27] V.S. Talanov, C.A. Regino, H. Kobayashi, M. Bernardo, P.L. Choyke, M.W. Brechbiel, Dendrimer-based nanoprobe for dual modality magnetic resonance and fluorescence imaging, Nano Lett. 6 (2006) 1459–1463.